Thermocapillary transport of energy during water evaporation

Fei Duan,[1] V. K. Badam,[2] F. Durst,[2] and C. A. Ward[1,*]
[1]*Thermodynamics and Kinetics Laboratory, Department of Mechanical and Industrial Engineering, 5 King's College Road, Toronto, Ontario, Canada M5S 3G8*
[2]*Institute of Fluid Mechanics, Friedrich-Alexander-University, Erlangen-Nürnberg Germany, Cauerstrasser 4, D-91058 Erlangen, Germany*
(Received 21 August 2004; revised manuscript received 21 March 2005; published 2 November 2005)

When evaporation occurs at a spherical water-vapor interface maintained at the circular mouth of a small funnel, studies of the energy transport have indicated that thermal conduction alone does not provide enough energy to evaporate the liquid at the observed rate. If the Gibbs model of the interface is adopted and the "surface-thermal capacity" is assigned a value of 30.6 ± 0.8 kJ/(m^2 K), then for evaporation experiments with the interfacial temperature in the range $-10\ ^\circ\mathrm{C} \leqslant T^{LV} \leqslant 3.5\ ^\circ\mathrm{C}$ and Marangoni number (Ma) in the range $100 < \mathrm{Ma} < 22{,}000$, it was found that if energy transport by both thermocapillary convection and thermal conduction were taken into account, conservation of energy was fully satisfied. The question addressed herein is whether the assigned value of the surface-thermal capacity is an *ad hoc* empirical parameter or a property of the water-vapor interface that can be used in other circumstances. Accordingly, a series of experiments has been conducted in which water evaporated at cylindrical interfaces that were, on average, 4.4 times larger in area than that of the spherical interfaces used to measure the surface-thermal capacity initially. It is shown that using the value of the surface-thermal capacity determined at a spherical interface, the energy transported by thermocapillary convection and thermal conduction at a cylindrical interface is sufficient to evaporate the liquid at the observed rate. Knowing the value of the surface-thermal capacity also allows the local evaporation flux to be calculated from the measured temperature profiles in the liquid and vapor phases. The calculated local evaporation flux can then be used with statistical rate theory to calculate the vapor-phase pressure along the interface. The predicted mean vapor-phase pressure is in close agreement with that measured, and the predicted pressure gradient is consistent with that expected when thermocapillary convection is present.

DOI: 10.1103/PhysRevE.72.056303 PACS number(s): 47.20.Dr

I. INTRODUCTION

Studies of energy transport to a spherical water-vapor interface maintained at the mouth of a circular stainless-steel funnel while the water evaporates under conditions that ensure the absence of buoyancy-driven convection in both the liquid and vapor phases have indicated that three steady-state, energy-transport regimes can be defined using the Marangoni number [1] as the defining parameter [2,3].

In the first, when the evaporation rate is small enough so that Ma is less than ~100, the interface is quiescent and thermal conduction to the interface (Stefan condition) provides the energy transport required to evaporate the liquid at the observed rate.

The second regime occurs when $100 < \mathrm{Ma} < 22{,}000$. This regime can be reached by lowering the pressure in the vapor phase while maintaining the temperature of water entering the funnel throat at a value just less than 4 °C. The lower pressure increases the evaporation rate and cools the liquid phase at the interface. Since water has its maximum density at 4 °C and the density decreases monotonically with further decreases in temperature, the temperature field ensured that there was no buoyancy-driven convection. Thermocapillary convection was present and gave rise to a uniform-temperature layer [2,3] immediately below the interface. In this regime, thermal conduction no longer provides sufficient energy transport to evaporate the liquid at the observed rate. Since the temperature at the funnel throat was constant, thermal energy was conducted through the stainless-steel funnel to the funnel rim where the liquid was heated. This produced a parabolic temperature field at the liquid-vapor interface, with the higher temperature at the funnel rim and minimum on the center line. It is this temperature profile that produced the thermocapillary convection. But since there is no buoyancy-driven convection in the liquid bulk, the type of convection produced when both thermocapillary and buoyancy-driven (Marangoni-Bénard) convection [4] are active was not present in the experiments.

A method of analyzing the energy transport in this regime has been proposed [3]. It is based on the Gibbs [5] dividing-surface approximation and leads to the definition of an excess property that represents the thermal capacity per unit area of the interface: if n^{LV} is the excess moles per unit area, u^{LV} the internal energy per excess mole, and c^{LV} the specific heat of the excess moles, then the "surface-thermal capacity" is the product $n^{LV}c^{LV}$ and is denoted as c_σ [3].

When the energy transported to the interface by thermocapillary convection and thermal conduction are equated to the energy required to evaporate the liquid at the observed rate, one finds that the value of the surface-thermal capacity can be determined from a measurement of the evaporation rate and the temperature profiles in the liquid and vapor phases [3]. In each of nine experiments in which $100 < \mathrm{Ma} < 22{,}000$ and the average evaporation flux $\overline{j_{ev}}$ was in the range $0.10\ \mathrm{g/(m^2\ s)} \leqslant \overline{j_{ev}} \leqslant 3.38\ \mathrm{g/(m^2\ s)}$, the surface-

*Corresponding author. FAX: 416-978-7322. Electronic address: ward@mie.utoronto.ca

thermal capacity was found to have the same value 30.6 ± 0.8 kJ/(m^2 K).

In the third regime Ma $>$ 22,000 the interfacial flow is turbulent and viscous dissipation is important [2,3]. Once the value of the surface-thermal capacity had been determined from the experiments conducted in the second regime, its value was used in the third regime to determine the viscous dissipation [3]. The viscous dissipation determined in this way for the turbulent interfacial convection was found to increase almost linearly with the maximum thermocapillary-generated interfacial speed.

Since the surface-thermal capacity was found to be constant over a wide range of experimental conditions, the results suggest that c_σ is a property of water that is defined in terms of the Gibbs dividing-surface approximation. However, the possibility exists that the value obtained for c_σ is *ad hoc*: since in each of the nine experiments the water-vapor interface was very nearly spherical, the interfacial curvature had approximately the same value in all experiments, 0.151 ± 0.003 mm^{-1}, and the value of c_σ is larger than one would expect for an equilibrium interface [3]. The objective of this study is to treat surface-thermal capacity as a property of water that does not change significantly when the interfacial temperature T^{LV} is in the range $-12\ ^\circ\mathrm{C} \leqslant T^{LV} \leqslant 3.5\ ^\circ\mathrm{C}$ and then to use this property in a predictive sense.

To determine if c_σ can be used in this way, a series of experiments has been performed in which water was maintained at the rectangular mouth of a stainless-steel channel while evaporating under steady-state conditions. This gives a cylindrically shaped interface. The interfacial temperature T^{LV} was in the range where the surface-thermal capacity is expected to be unchanging; the Marangoni number was in the range 5,800 $<$ Ma $<$ 22,000—thus the experiments were in the second or third regimes—but in contrast with the experiments of [3], the shape of the water-vapor interface was cylindrical. This changed the curvature to 0.109 ± 0.014 mm^{-1} in one direction and zero in the other.

More importantly, the area of the cylindrical interface was increased by, on average, a factor of 4.4, compared to that of the spherical interfaces that were used to measure c_σ. Before the interface becomes turbulent, the measured value of the thermocapillary energy transport reaches $\sim$50% of the total required to evaporate the liquid at the measured rate. Thus, if there were a significant error in the value of c_σ, it would have been clearly seen when the predictions were compared with measurements. Using the previously recorded value of c_σ, it is shown that the predicted values of the thermocapillary convection and thermal conduction sum to give the energy transport required to evaporate the liquid at the measured rate. Thus we did not identify any error in the value of c_σ—above the $\pm 2.5\%$ suggested in [3]—from the comparisons made at the cylindrical interface.

The value of surface-thermal capacity is examined further by using it to calculate the local evaporation flux j_{ev}. Depending on the total evaporation rate, we find that j_{ev} can be strongly nonuniform. The measured values of the interfacial temperatures in the liquid and vapor phases, T_I^L and T_I^V, and the values of j_{ev} may be used with statistical rate theory (SRT) [6–20] to predict the local vapor-phase pressure along the interface. Since SRT introduces no fitting parameters, the predicted pressure can be compared directly with that measured. The calculated mean of the vapor-phase pressures on the liquid-vapor interface is found to be in agreement with the measured value of the vapor-phase pressure, but perhaps more importantly, the local pressure along the interface can be calculated as a function of position and the predicted pressure gradient is consistent with that expected when thermocapillary flow is present in the direction indicated by the measured temperature profile.

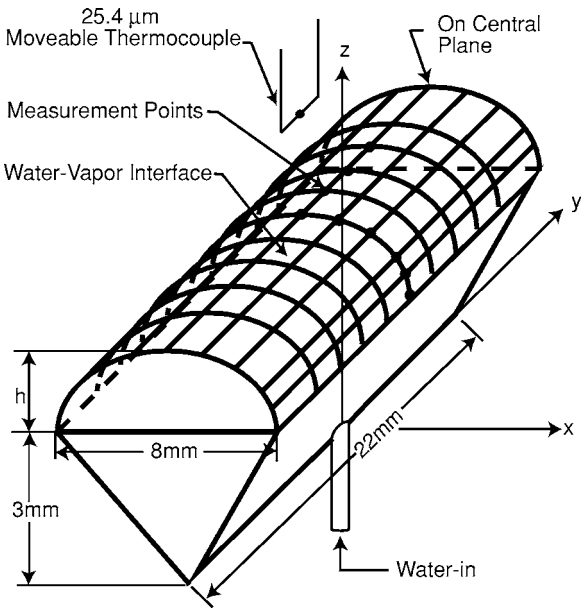

FIG. 1. Schematic of the stainless-steel channel used in the study. Note the rectangular mouth of the channel. As a result, water at the channel mouth formed a cylindrical surface.

II. EXPERIMENTAL METHODS AND RESULTS

The experimental apparatus has been previously described [21] and is similar to the ones used in [2,3]. The important difference is that the funnel, with its circular mouth, used in [2,3] is replaced by the stainless-steel, V-shaped channel with a rectangular mouth. It is shown schematically in Fig. 1.

In preparation for an experiment, purified water (resistivity 18.0$M\Omega$-cm) was placed in a glass flask. The vapor phase of the flask was connected through a valving system to a mechanical vacuum pump that allowed the water to be degassed and then transferred through a stainless-steel tube directly into a syringe that was mounted in a pump. Water could be pumped from the syringe into the bottom of the stainless-steel channel that was enclosed in a vacuum chamber. A (type-K, sheathed, 25.4-μm-diam) thermocouple was placed inside the tube with the bead at the junction of the tube and the channel. A separate cooling system could bring the temperature at this position to a chosen value. The values chosen for each experiment are listed in Table I. The chamber was connected to two pumping systems: one was a turbomolecular and associated backing pump, and the other was a mechanical vacuum pump. As indicated in Fig. 1, when water filled the channel, the interface was cylindrically

TABLE I. Thermal conditions measured in three dimensions during steady state.

Experiment:	EvC1	EvC2	EvC3	EvC4	EvC5
Vapor-phase pressure (Pa)	661.3±13.3	551.9±13.3	469.3±13.3	317.3±13.3	256.0±13.3
Max. intf. height above channel mouth (mm)	1.00±0.01	1.00±0.01	0.70±0.01	1.00±0.01	0.91±0.01
Avg. evap. flux (g/m^2 s)	0.92±0.01	1.52±0.02	1.64±0.02	3.26±0.03	3.48±0.04
Throat temperature (°C)	3.52±0.05	3.52±0.05	3.67±0.05	3.62±0.05	3.67±0.06
Unif. temp. layer[a] (mm)	0.090±0.015	0.095±0.010	0.075±0.010	0.055±0.010	0.025±0.010
Marangoni No.	5,831	11,186	13,602	20,778	22,012
Max. tangential speed (mm/s)	0.766±0.027	0.782±0.056	0.721±0.016	0.852±0.018	0.931±0.016
Interfacial radius r_0 (mm)	8.50±0.09	8.50±0.09	11.78±0.12	8.50±0.09	9.25±0.09
Est. error: total energy transport to interface (%)	±2.4	±4.8	±2.0	±2.0	±2.5
Intf. vap. temp. (°C) $\varphi=\arcsin(0.0/r_0)$	2.40±0.02	−0.06±0.02	−1.86±0.03	−7.01±0.02	−9.78±0.02
Intf. liq. temp. (°C) $\varphi=\arcsin(0.0/r_0)$	1.13±0.02	−1.45±0.02	−3.41±0.02	−8.63±0.02	−11.65±0.02
Intf. vap. temp. (°C) $\varphi=\arcsin(1.0/r_0)$	2.23±0.02	−0.20±0.02	−1.84±0.03	−6.99±0.02	−9.81±0.02
Intf. liq. temp. (°C) $\varphi=\arcsin(1.0/r_0)$	1.17±0.02	−1.48±0.02	−3.34±0.02	−8.57±0.02	−11.79±0.02
Intf. vap. temp. (°C) $\varphi=\arcsin(2.0/r_0)$	2.27±0.02	−0.09±0.02	−1.71±0.02	−6.92±0.02	−9.75±0.02
Intf. liq. temp. (°C) $\varphi=\arcsin(2.0/r_0)$	1.19±0.02	−1.48±0.02	−3.31±0.02	−8.49±0.02	−11.68±0.02
Intf. vap. temp. (°C) $\varphi=\arcsin(3.0/r_0)$	2.18±0.02	−0.12±0.02	−1.67±0.02	−6.81±0.02	−9.59±0.02[b]
Intf. liq. temp. (°C) $\varphi=\arcsin(3.0/r_0)$	1.17±0.02	−1.38±0.02	−3.11±0.02	−8.53±0.02	−11.66±0.02[b]
Intf. vap. temp. (°C) $\varphi=\arcsin(3.5/r_0)$	2.20±0.02	−0.11±0.02	−1.53±0.02	−6.58±0.02	−9.16±0.02
Intf. liq. temp. (°C) $\varphi=\arcsin(3.5/r_0)$	1.26±0.02	−1.39±0.02	−3.15±0.02	−8.26±0.02	−10.70±0.02

[a]On the central plane.
[b]At $\varphi=\arcsin(2.5/r_0)$.

shaped. A (type-K) thermocouple constructed of 25.4-μm-diam wires was formed into a U shape, with a horizontal section 3 mm in length and with the thermocouple bead—~50 μm in diameter—at the center. The thermocouple was mounted on a positioner that had a positioning accuracy of ±10 μm in any of the three dimensions and allowed the temperature to be measured in the liquid and vapor phases with an accuracy ±0.04 K. The positions on the interface where the temperature was measured are indicated in Fig. 1.

Before each experiment, the pressure in the vacuum chamber was reduced to 10^{-3} Pa by pumping with the turbomolecular pump for approximately 12 h. The prepared water was then pumped into the bottom of the channel and up to the rectangular mouth of the channel where the water-vapor interface was visible from outside the vacuum chamber. To prevent subsequent bubble formation, the pressure in the chamber was increased to ~2.5 bars and held at this value for approximately 30 min. Approximately ~4 ml of water was flushed out of the channel and into the chamber. The mechanical pump was then used to evacuate the chamber until it was dry.

The height of the liquid-vapor interface in each experiment above the channel mouth was limited to ~1 mm (Table I). When the measured height of the interface was compared with that calculated assuming the interface was cylindrical, the error in the height at the five polar positions in the middle of the cylinder indicated in Fig. 1 was less than 1.5% for any experiment; however, there was some error at the ends of the rectangular mouth that was closed by glass plates. A meniscus was present at each plate that caused a deviation from the cylindrical shape. This error is neglected in the analysis.

III. EXPERIMENTAL PROCEDURE AND RESULTS

The temperature at the entry to the channel was set at a value just less than 4 °C in each experiment—the temperature of maximum water density—and the evaporation at the interface cooled the water further so that the lightest water in the channel was at the highest point. Similarly, the coldest

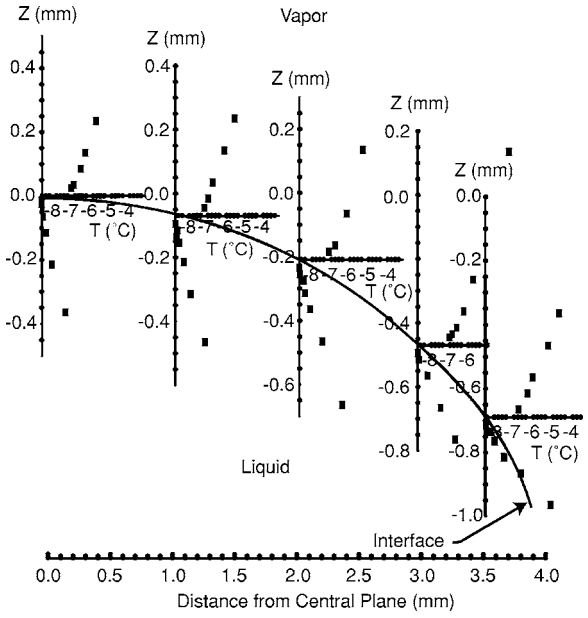

FIG. 2. Temperatures measured in the vertical direction at each of five horizontal distances from the central plane of the cylindrical water-vapor interface during experiment EvC4 (Table I).

vapor was at the liquid-vapor interface. Thus there was no buoyancy-driven convection in either phase. This technique to eliminate buoyancy-driven convection has been applied previously [2,3].

After the temperature at the channel entry had been set, the evacuation rate of the chamber and the syringe pumping rate were adjusted so the water injection rate into the channel was equal to the evaporation rate. As a result, the water-vapor interface was unmoving. The position of the interface could be monitored with a cathetometer from outside the vacuum chamber. Once the interface had been brought into steady state, it did not move by more ± 10 μm during the course of an experiment. During the steady-state period, the pressure was measured with a manometer at a position ~ 10 cm above the mouth of the channel. With water evaporating under steady-state conditions and the other experimental variables set (Table I), the moveable thermocouple was used to measure the temperature profile as a function of vertical distance at each of the nine points indicated in Fig. 1.

The results obtained on the central plane of a cylindrical water-vapor interface in the middle of the channel mouth and at four horizontal distances from the central plane in one horizontal direction, during EvC4 (Table I), are shown in Fig. 2. Note that at each position, the interfacial vapor temperature was found to be greater than the interfacial liquid temperature, as has been found in other experiments [2,3,6–10,21]; there was a thin liquid layer immediately below the interface in which the temperature was uniform; and below the uniform-temperature layer, the temperature increased linearly with depth [2,3,6]. As will be seen, the thickness of the uniform-temperature layer is an important parameter used to determine the thermocapillary flow rate [2]. The value of this parameter was determined by immersing the thermocouple bead in the liquid just below the interface and moving it to successively greater depths in

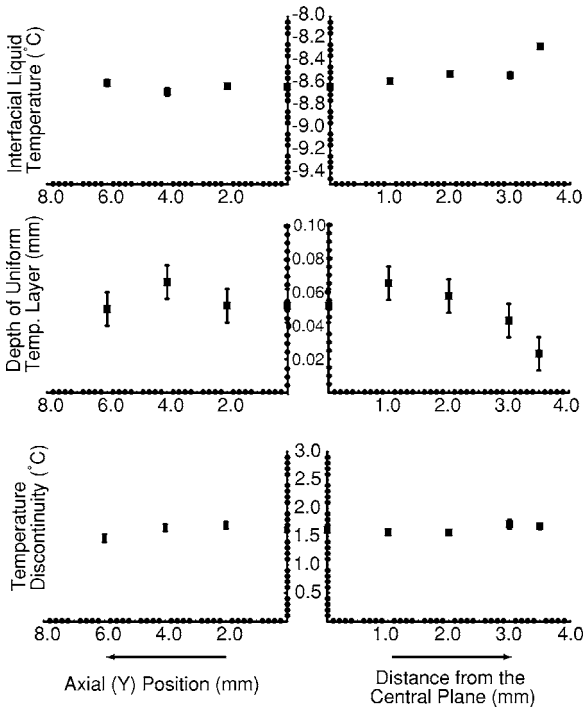

FIG. 3. Measurements during EvC4 (Table I) of (three left-hand graphs) the interfacial liquid temperature, the depth of the uniform-temperature layer, and the magnitude of the interfacial temperature discontinuity plotted as a function of the axial position. However, in a direction perpendicular to the central plane and in the middle of the channel, the temperature as a function of position (upper graph), the depth of the uniform temperature layer (middle graph), and the magnitude of the temperature discontinuity are shown as a function of the distance from the central plane of the cylindrical water-vapor interface.

~ 20-μm steps. In a series of readings at different positions, the temperature values were found not to be statistically different. The thickness of the uniform-temperature layer is determined by the depth for which this relation is maintained.

As indicated in Fig. 3, the temperature field was almost unchanging with axial position, but as a function of distance from the central plane the temperature increased, reaching a maximum near the intersection of the water-vapor interface with the mouth of the channel.

IV. ANALYSIS OF EXPERIMENTAL RESULTS

The Marangoni number was used in [3] to describe the flow regimes produced by thermocapillary convection. If the surface tension is denoted by γ^{LV}, the temperature of the water at the entry to the channel by T_t^L, the temperature on the central plane at the liquid-vapor interface by T_{0I}^L, the thermal diffusivity of the liquid by α_L, the dynamic viscosity by η, and the vertical distance from the throat thermocouple to the liquid-vapor interface on the central plane by D, then the Marangoni number can be expressed

$$\mathrm{Ma} = \left(\frac{\partial \gamma^{LV}}{\partial T} \right)_I \frac{(T_{0I}^L - T_t^L) D}{\alpha_L \eta}. \tag{1}$$

The values of Ma for each experiment are given in Table I, and in Fig. 4, the values of the Ma for the experiments de-

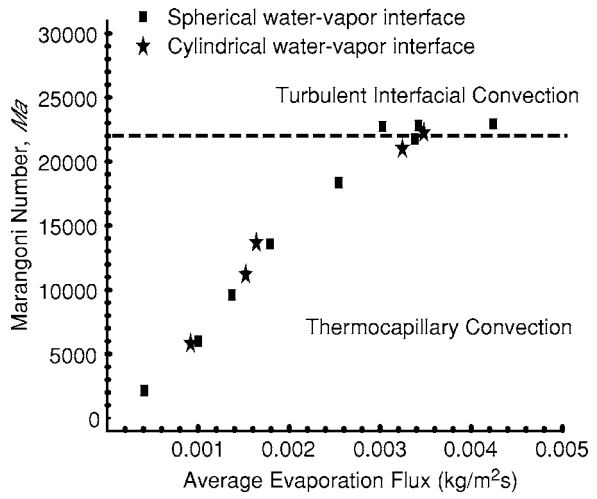

FIG. 4. The Marangoni number of the evaporation experiments conducted with a cylindrical water-vapor interface compared with that of the experiments performed using a spherical interface [3]. Note that four of the five experiments described in Table I were such that $\mathrm{Ma} < 22{,}000$ and therefore were expected to be in the second regime of interfacial flow (see the Introduction).

scribed in Table I are compared with those of the experiments in which water evaporated at a spherical water-vapor interface [3]. Note that four of the five experiments described in Table I were such that $100 < \mathrm{Ma} < 22{,}000$ and Ma for the other one had a value greater than 22,000. Thus, EvCl–EvC4 are expected to be in the second regime where, for evaporation from a spherical interface, thermal conduction to the interface does not supply sufficient energy to evaporate the liquid at the observed rate; the remainder of the energy transport is expected to be supplied by thermocapillary convection. Also, in this regime, viscous dissipation is negligible.

To investigate the second regime when evaporation occurs at a cylindrically shaped interface, we again adopt the Gibbs dividing-surface approximation and treat the interface region as consisting of three phases: liquid, vapor, and interface. As indicated in [3], in this approximation the internal energy per excess mole, u^{LV}, may be expressed in terms of the excess entropy per unit surface area, σ^{LV}, and the surface area per excess mole, α^{LV}. Note that the latter is the inverse of the number of excess moles n^{LV} per unit surface area:

$$du^{LV} = T^{LV} d\sigma^{LV} + \gamma^{LV} d\alpha^{LV}. \tag{2}$$

A Helmholtz function for the surface phase, f^{LV}, may be defined as

$$f^{LV} \equiv u^{LV} - T^{LV}\sigma^{LV}; \tag{3}$$

then,

$$df^{LV} = -\sigma^{LV} dT^{LV} + \gamma^{LV} d\alpha^{LV}. \tag{4}$$

From Eq. (4), it follows that f^{LV} has as its independent variables T^{LV} and α^{LV} and that σ^{LV} can be expressed in terms of these same variables. It then follows from Eq. (3) that

$$u^{LV} = u^{LV}(T^{LV}, \alpha^{LV}). \tag{5}$$

We shall make use of Eq. (5) below.

The velocity in either bulk phase is denoted as $\boldsymbol{\nu}^{\alpha}$, where α is L or V, and the velocity on the interface by $\boldsymbol{\nu}^{LV}$. We shall approximate the interface as cylindrical with radius r_0 and use cylindrical coordinates φ and y to define a position on the interface. Under steady-state conditions, the molar flux to the interface must equal that, leaving

$$n^L \boldsymbol{\nu}_I^L \cdot \boldsymbol{i}_r = n^V \boldsymbol{\nu}_I^V \cdot \boldsymbol{i}_r + \boldsymbol{\nabla}(n^{LV}\nu_{\varphi}^{LV}) \cdot \boldsymbol{i}_{\varphi} + \boldsymbol{\nabla}(n^{LV}\nu_y^{LV}) \cdot \boldsymbol{i}_y, \tag{6}$$

where the subscript I on a quantity indicates it is to be evaluated at the interface. We take the evaporation flux to be given by

$$j_{ev} = n^L \boldsymbol{\nu}_I^L \cdot \boldsymbol{i}_r = n^V \boldsymbol{\nu}_I^V \cdot \boldsymbol{i}_r. \tag{7}$$

Then Eq. (6) reduces to

$$\boldsymbol{\nabla}(n^{LV}\nu_{\varphi}^{LV}) \cdot \boldsymbol{i}_{\varphi} + \boldsymbol{\nabla}(n^{LV}\nu_y^{LV}) \cdot \boldsymbol{i}_y = 0. \tag{8}$$

Also, under steady-state conditions the net energy transported into a surface element must go into the change of phase or viscous dissipation:

$$\begin{aligned}(n^L h^L \boldsymbol{\nu}^L - \kappa^L \boldsymbol{\nabla} T^L)_I \cdot \boldsymbol{i}_r = {} & (n^V h^V \boldsymbol{\nu}^V - \kappa^V \boldsymbol{\nabla} T^V)_I \cdot \boldsymbol{i}_r + \Phi_I \\ & + [n^{LV}\nu_{\varphi}^{LV}(\boldsymbol{\nabla} u^{LV})_I \\ & + u^{LV} \boldsymbol{\nabla} (n^{LV}\nu_{\varphi}^{LV})_I] \cdot \boldsymbol{i}_{\varphi} \\ & + [n^{LV}\nu_y^{LV}(\boldsymbol{\nabla} u^{LV})_I \\ & + u^{LV}(\boldsymbol{\nabla}(n^{LV}\nu_y^{LV}))_I] \cdot \boldsymbol{i}_y. \end{aligned} \tag{9}$$

After combining Eqs. (7) and (8) with Eq. (9),

$$\begin{aligned}(\kappa^V \boldsymbol{\nabla} T^V - \kappa^L \boldsymbol{\nabla} T^L)_I \cdot \boldsymbol{i}_r = j_{ev}(h^V - h^L)_I + \Bigg(& \frac{n^{LV}\nu_{\varphi}^{LV}}{r_0}\left(\frac{\partial u^{LV}}{\partial \varphi}\right)_y \\ & + (n^{LV}\nu_y^{LV})\left(\frac{\partial u^{LV}}{\partial y}\right)_{\varphi} + \Phi \Bigg)_I. \end{aligned} \tag{10}$$

The specific heat of the surface phase, c^{LV}, is given by

$$c^{LV} = \left(\frac{\partial u^{LV}}{\partial T}\right)_{\alpha^{LV}}. \tag{11}$$

If use is made of Eqs. (5) and (11), then Eq. (10) may be written

$$\begin{aligned}(\kappa^V \boldsymbol{\nabla} T^V - \kappa^L \boldsymbol{\nabla} T^L)_I \cdot \boldsymbol{i}_r & \\ = j_{ev}(h^V - h^L)_I + \frac{n^{LV}\nu_{\varphi}^{LV}}{r_0}\Bigg(& c^{LV}\left(\frac{\partial T^{LV}}{\partial \varphi}\right)_y + \gamma^{LV}\left(\frac{\partial \alpha^{LV}}{\partial \varphi}\right)_y\Bigg)_I \\ + (n^{LV}\nu_y^{LV})\Bigg(& c^{LV}\left(\frac{\partial T^{LV}}{\partial y}\right)_{\varphi} + \gamma^{LV}\left(\frac{\partial \alpha^{LV}}{\partial y}\right)_{\varphi}\Bigg)_I + \Phi_I. \end{aligned} \tag{12}$$

We neglect any variation in α^{LV} with position on the interface, and in view of the results shown in Fig. 3, any variation in T^{LV} with changes in axial position y. Also, we take T^{LV} and $\boldsymbol{\nu}^{LV}$ to have the same value T_I^L and $\boldsymbol{\nu}_I^L$, respectively. After making use of the definition of c_{σ}, Eq. (12) may then be simplified to

$$j_{ev}(h^V - h^L)_I = (\kappa^V \boldsymbol{\nabla} T^V - \kappa^L \boldsymbol{\nabla} T^L)_I \cdot \boldsymbol{i}_r - \frac{c_{\sigma}\nu_{\varphi}^{LV}}{r_0}\left(\frac{dT_I^L}{d\varphi}\right) - \Phi_I. \tag{13}$$

There was, as indicated in Fig. 3, a gradient of T_I^L in the $\boldsymbol{i}_\varphi$ direction. To determine the thermocapillary flow in that direction, ν_φ^{LV}, we follow the method proposed in [2] for evaporation at a spherical interface and equate the gradient in surface tension in that direction to the viscous stress in that direction. After neglecting the dependence ν_r^L on φ, this condition gives

$$\frac{1}{r_0}\left(\frac{d\gamma^{LV}}{dT_I^L}\right)\left(\frac{dT_I^L}{d\varphi}\right)=\eta\left(\frac{\partial \nu_\varphi^L}{\partial r}-\frac{\nu_\varphi^L}{r}\right)_I. \tag{14}$$

Except for the change of variable definition, this is the same form of equation as obtained in [2]; thus, the same procedure may be used to determine the approximate solution:

$$\nu_\varphi^{LV}=\left(-\frac{1}{\eta}\right)\left(\frac{d\gamma^{LV}}{\partial T_I^L}\right)\left(\frac{dT_I^L}{d\varphi}\right)\ln\left(1-\frac{\delta_u}{r_0}\right), \tag{15}$$

where δ_u is the thickness of the uniform-temperature layer. As seen in Fig. 3, δ_u depends on φ, but shows little dependence on y. The transport of energy at the interface is governed by Eqs. (13) and (15).

Energy transport to the interface

For the nonturbulent experiments ($\mathrm{Ma}<22{,}000$), the viscous dissipation is negligible, and since the variation of $(h^V-h^L)_I$ in any particular experiment was less than 1%, when Eq. (13) is integrated over the interface, one finds

$$J_{ev}(h^V-h^L)_I=2l_m r_0\int_0^{\varphi_m}\left[\kappa^V\left(\frac{\partial T^V}{\partial r}\right)_I-\kappa^L\left(\frac{\partial T^L}{\partial r}\right)_I\right]d\varphi - (2l_m c_\sigma)\int_0^{\varphi_m}\nu_\varphi^{LV}\left(\frac{\partial T^L}{\partial \varphi}\right)_I d\varphi, \tag{16}$$

where the length of the rectangular mouth opening is l_m and φ_m is the maximum value of the polar angle. If $2r_m$ is the width of the mouth opening, then

$$\varphi_m=\arcsin\left[\frac{r_m}{r_0}\right], \tag{17}$$

and we have assumed the properties are symmetric about a central plane through $\varphi=0$.

For each experiment, the value of the energy required to evaporate the liquid at the observed rate, $J_{ev}(h^V-h^L)_I$, may be determined in two ways: one is to measure the values of J_{ev} and use the known values of the enthalpies; the other is to calculate the value of the terms on the left-hand side of Eq. (16). To make this calculation, the value of surface-thermal capacity c_σ must be used, and we shall use the value determined for a spherical interface in [3]. By comparing the value of $J_{ev}(h^V-h^L)_I$ determined in these two ways, we may determine if the surface-thermal capacity behaves as a property of the water-vapor interface.

We first consider a method by which the measurements may be used to calculate $J_{ev}(h^V-h^L)_I$ using Eq. (16). The measured interfacial temperatures and the depth of the uniform-temperature layer are each such that they may be described by the same type of equations:

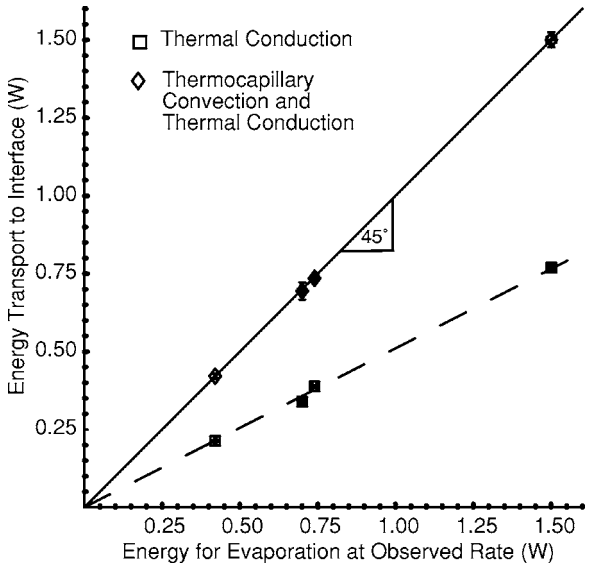

FIG. 5. Comparison of the energy required to evaporate the liquid at the measured rate with that calculated by thermal conduction alone (dashed line) and that calculated by thermal conduction and thermocapillary convection (solid, 45° line). The calculated amount by thermocapillary convection is based on c_σ having a value 30.6 kJ/(m^2 K). Note that at the higher evaporation rate, thermal conduction accounts for only ~50% of the total energy transport rate.

$$T^{LV}=a_0+a_1\sin^4\varphi, \tag{18}$$

$$\delta_u=b_0+b_1\sin^4\varphi, \tag{19}$$

where the constants (a_0,b_0,a_1,b_1) are determined numerically for each experiment. We note that the empirical relations given in Eqs. (18) and (19) for the cylindrically shaped interface are different than the corresponding ones used for the spherical interface [3].

The local thermal conduction to the interface from the liquid and vapor phases can be determined from temperature measurements, such as those shown in Fig. 2:

$$\kappa^V\left(\frac{\partial T^V}{\partial r}\right)_I-\kappa^L\left(\frac{\partial T^L}{\partial r}\right)_I=\frac{1}{\cos\varphi}\left[\kappa^V\left(\frac{\partial T^V}{\partial z}\right)_I-\kappa^L\left(\frac{\partial T^L}{\partial z}\right)_I\right], \tag{20}$$

and we find that

$$\kappa^V\left(\frac{\partial T^V}{\partial r}\right)_I-\kappa^L\left(\frac{\partial T^L}{\partial r}\right)_I=c_0+c_1\cos\varphi+c_2\cos^2\varphi+c_3\cos^3\varphi, \tag{21}$$

where $c_j(0\leqslant j\leqslant 3)$ are constants that may be determined for each experiment. When Eqs. (18), (19), and (20) are used in Eq. (16) and c_σ is assigned the value 30.6 kJ/(m^2 K) [3], one calculates the values of $J_{ev}(h^V-h^L)_I$ shown in Fig. 5 for each of the nonturbulent experiments. The error bars in the thermal conduction, $\Delta(\dot{Q}_N)$, results from the error in the measured position, $\Delta(r)$, error in the measured temperature,

$\Delta(mT^{LV})$, and the error in the fitting relations or calculated temperature, $\Delta(cT^{LV})$. Then [22,23],

$$\Delta(\dot{Q}_N) = \sqrt{[\Delta(r)]^2 + [\Delta(mT^{LV})]^2 + [\Delta(cT^{LV})]^2}. \quad (22)$$

Similarly, the error in the thermocapillary convection, $\Delta(TC)$ [see Eq. (16)], is taken to result from the error in $\Delta(c_\sigma)$, in the thermocapillary speed, $\Delta(\nu_\varphi^{LV})$, and $\Delta(\partial T_I^L/\partial\varphi)$:

$$\Delta(TC) = \sqrt{\Delta(c_\sigma)^2 + \Delta(\nu_\varphi^{LV})^2 + \Delta(\partial T_I^L/\partial\varphi)^2}. \quad (23)$$

The estimated error in c_σ obtained in [3] was ±2.5%. We take the same value for the error in c_σ at the cylindrical interface. Then the error in the calculated total energy transport to the interface is the sum of the error in the thermal conduction and the thermocapillary convection. The values of the estimated errors in the total energy flux to the interface in each of the experiments are listed in Table I.

As may be seen from Fig. 5, there was no measured disagreement between the sum of the energy transported by thermocapillary convection and thermal conduction and the energy required to evaporate the liquid at the observed rate. Also, when the liquid was evaporating at the highest rate, we note that the energy supplied by the thermal conduction only accounts for ~50% of the total. Since in these experiments the area of the liquid-vapor interface was on average 4.4 times larger than the area of spherical interface used to measure the value of c_σ, but nonetheless the predicted total energy transport based on the value of c_σ satisfies the energy conservation principle, the results suggest that the recorded value of c_σ is not in error by more than ±2.5%.

Only one of the experiments was in the turbulent regime (Ma > 22,000). It has been previously found that in this regime, the character of the interfacial flow changes and the viscous dissipation becomes non-negligible [2,3]. Since the value of the surface-thermal capacity has been established, we may follow the procedure of [3] to determine the value of the viscous dissipation averaged over the surface, $\bar{\Phi}_I$:

$$\bar{\Phi}_I = \left(\frac{1}{\varphi_m}\right)\int_0^{\varphi_m}\left[\kappa^V\left(\frac{\partial T^V}{\partial r}\right)_I - \kappa^L\left(\frac{\partial T^L}{\partial r}\right)_I - \frac{c_\sigma \bar{\nu}_\varphi^{LV}}{r_0}\left(\frac{dT_I^L}{d\varphi}\right)\right]d\varphi - \frac{J_{ev}(h^V - h^L)_I}{2l_m r_0 \varphi_m}. \quad (24)$$

The value of $\bar{\Phi}_I$ for EvC5 (Table I) is shown in Fig. 6 where it may be compared with that obtained at the spherical interface. The results there indicate that when the maximum thermocapillary speed has the same value at a spherical interface as at a cylindrical interface and the interfacial flow is turbulent in both cases, the viscous dissipation is larger at the spherical interface.

V. PREDICTION OF THE VAPOR-PHASE PRESSURE

The fact that the value of the surface-thermal capacity c_σ determined from the study of evaporation at a spherical water-vapor interface can be applied to predict the energy transport by thermocapillary convection at a cylindrical interface supports the hypothesis that this quantity is a property

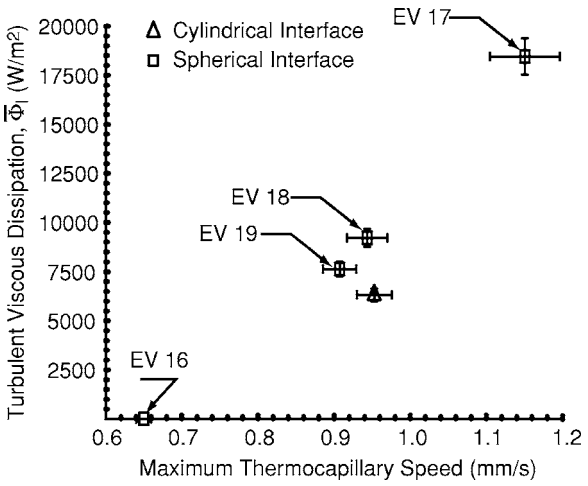

FIG. 6. Comparison of the viscous dissipation at a spherical interface [3] (EV16–EV19) and at a cylindrical interface once the interfacial flow becomes turbulent.

of the water-vapor interface when the Gibbs dividing-surface approximation is used to define the interface region. This result can be examined further by first using Eq. (13) to calculate the local evaporation flux and then using statistical rate theory to calculate the local vapor-phase pressure.

From Eqs. (13), (15), (18), and (19), one finds the local evaporation fluxes j_{ev} shown in Fig. 7 for each experiment. Note that the evaporation flux is strongly nonuniform, especially at the higher evaporation rates, and that the maximum occurs near the solid surface.

The expression for the evaporation flux may be obtained from statistical rate theory [7,11,12]. If the evaporation process is taking place in an isolated system, statistical rate theory gives the expression for the evaporation flux at one instant, in terms of a virtual change in the entropy at that

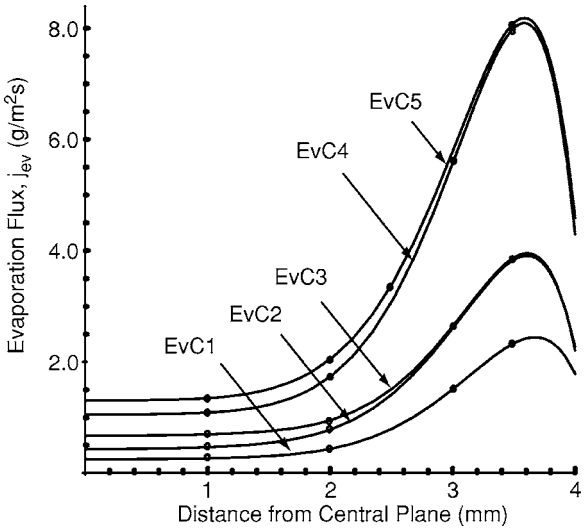

FIG. 7. Calculated local evaporation flux assuming that the surface-thermal capacity c_σ has a value of 30.6 kJ/(m² K) in each of the five experiments being considered (Table I). The solid circles indicate the values calculated at the measurement point of each experiment.

instant that results from one molecule going from the liquid to the vapor phase, Δs_{LV} the Boltzmann constant k_B, and the equilibrium exchange flux that would exist between the liquid and vapor phases when the isolated system finally evolved to equilibrium, K_e [7]:

$$j_{ev} = 2K_e \sinh(\Delta s_{LV}/k_B). \tag{25}$$

The change in the entropy may be expressed in terms of the chemical potentials μ^L and μ^V, the temperatures in each phase, and enthalpy in the vapor phase, h^V:

$$\Delta s_{LV} = \left(\frac{\mu^L}{T_I^L} - \frac{\mu^V}{T_I^V}\right) + h^V\left(\frac{1}{T_I^V} - \frac{1}{T_I^L}\right). \tag{26}$$

An approximate expression for Δs_{LV} can be obtained from statistical mechanics [7]:

$$\begin{aligned}\frac{\Delta s_{LV}}{k_B} &= 4\left(1 - \frac{T_I^V}{T_I^L}\right) + \left(\frac{1}{T_I^V} - \frac{1}{T_I^L}\right) \\ &\times \sum_{l=1}^{3}\left(\frac{\hbar\omega_l}{2k_B} + \frac{\hbar\omega_l/k_B}{\exp(\hbar\omega_l/k_B T_I^V) - 1}\right) + \frac{v_s^L(T_I^L)}{k_B T_I^L} \\ &\times \left(P_I^V + \frac{\gamma^{LV}(T_I^L)}{r_0} - P_s(T_I^L)\right) \\ &+ \ln\left[\left(\frac{T_I^V}{T_I^L}\right)^4\left(\frac{P_s(T_I^L)}{P_I^V}\right)\right] + \ln\left(\frac{q_{\rm vib}(T_I^V)}{q_{\rm vib}(T_I^L)}\right),\end{aligned} \tag{27}$$

where a subscript s indicates the property is to be evaluated at the saturation condition between a liquid and vapor phase across a flat surface and $q_{\rm vib}$ is the vibrational partition function. It may be written in terms of the fundamental vibration frequencies of the water molecule, ω_l $(1 \leqslant l \leqslant 3)$:

$$q_{\rm vib} = \prod_{l=1}^{3} \frac{\exp(-\hbar\omega_l/2k_B T_I)}{1 - \exp(-\hbar\omega_l/k_B T_I)}. \tag{28}$$

Their values of the frequencies have been measured: 1,590, 3,651, and 3,756 cm^{-1} [24]. We assume that when the isolated system evolves to equilibrium the interface can still be approximated as cylindrical with radius r_0 and the final temperature will be approximately the instantaneous interfacial liquid temperature. The equilibrium exchange rate is obtained from equality of the chemical potentials in the liquid phase. This leads to an equation that may be solved iteratively to determine the pressure in the liquid phase, P_{0e}^L, in the final equilibrium state of the isolated system:

$$P_{0e}^L = P_s(T^L)\exp\left[\frac{v_s^L}{k_B T_I^L}[P_{0e}^L - P_s(T_I^L)]\right] + \frac{\gamma^{LV}(T_I^L)}{r_0}. \tag{29}$$

The equilibrium exchange rate then is given by

$$K_e = \frac{P_s(T_I^L)\exp\left(\frac{\nu_s^L}{k_B T^L}[P_{0e}^L - P_s(T_I^L)]\right)}{\sqrt{2\pi m k_B T_I^L}}. \tag{30}$$

If the values of T_I^L, T_I^V, j_{ev}, and r_0 are given at one instant, Eqs. (25)–(30) constitute a coupled system, with no adjustable parameters, that can be used to predict the vapor-phase pressure at a point on the liquid-vapor interface at the instant considered. In the isolated system, the properties would evolve to other values with time. However, we assume that if the instantaneous values of T_I^L, T_I^V, j_{ev}, and r_0 are the same in a steady-state system and in the isolated system at one instant, then at that instant the vapor-phase pressure will have the same value in the two systems.

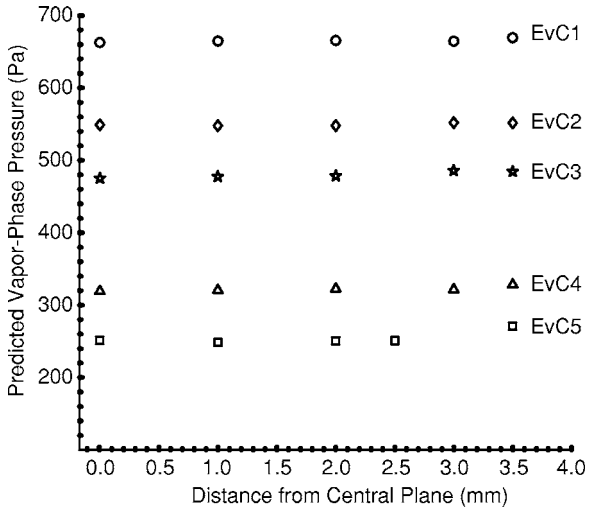

FIG. 8. Values of the local vapor-phase pressure on the liquid-vapor interface in each of the experiments predicted from statistical rate theory with the value of the surface-thermal capacity c_σ taken to be 30.6 $\mathrm{kJ/(m^2\,K)}$ in the calculations.

This allows the vapor-phase pressure at each measurement point on the liquid-vapor interface to be predicted. The values of the interfacial liquid and vapor temperatures at each measurement point and the radius of the liquid-vapor interface for each experiment are listed in Table I, and the values of the local evaporation flux is shown in Fig. 7. When these values are used in Eqs. (25)–(30), one finds the values of the local vapor-phase pressures that are shown in Fig. 8 for each of the five experiments. The pressure is slightly higher near the intersection of the water-vapor interface with the channel mouth than on the central plane of the water-vapor interface. This is physically reasonable, since the thermocapillary flow is toward the central plane of the water-vapor interface (see Fig. 3). However, a more rigorous test is to compare the average pressure on the interface with that measured in the vapor phase during the steady-state period of each experiment. The averages of the calculated values are shown in Fig. 9 where they may be compared with the measured values of the vapor-phase pressure. The error bars on the measurements of the vapor-phase pressure are taken to be ±13.3 Pa, the reading error of the manometer. The very close agreement between the predicted and measured pressures indicates that the calculated local flux obtained from the value of surface-thermal capacity leads to an accurate prediction of the pressure. This supports treating c_σ as a property and indicates that for water its value is near 30.6 $\mathrm{kJ/(m^2\,K)}$ when $-12\ ^\circ\mathrm{C} \leqslant T^{LV} \leqslant 3.5\ ^\circ\mathrm{C}$.

VI. DISCUSSION AND CONCLUSION

The water at the rectangular mouth of the stainless-steel channel (see Fig. 1) formed a cylindrically shaped interface.

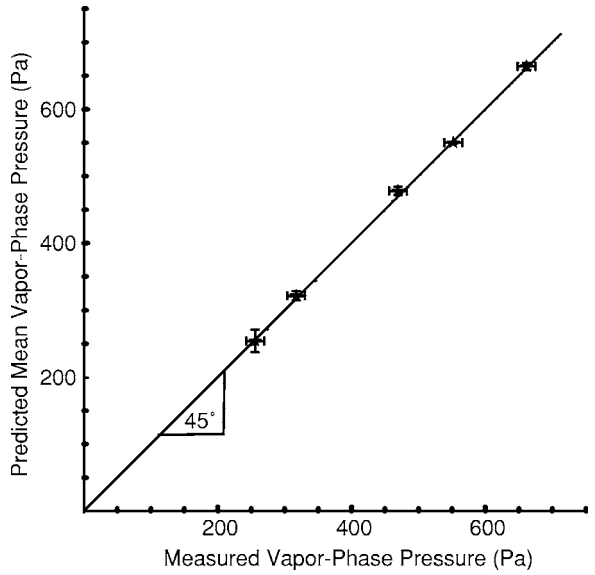

FIG. 9. Comparison of the measured vapor-phase pressure with the mean vapor-phase pressure predicted from statistical rate theory with the surface-thermal capacity c_σ taken to have a value of 30.6 kJ/(m^2 K).

The temperature of the water entering the rectangular channel was slightly less than 4 °C and colder still at the liquid-vapor interface. Since water has it maximum density at 4 °C, the temperature field ensured that there was no buoyancy-driven convection in the liquid phase, as the water evaporated under steady-state conditions [2,3,21].

If one imagines a plane through the center line of the cylindrical interface and the rectangular mouth of the channel, the interfacial temperature field changed negligibly with axial position, but in the direction perpendicular to the plane, the temperature field was parabolic. Thermal conduction through the wall of the stainless-steel channel heated the liquid at the channel rim, and since the thermal conductivity of stainless steel is more than 20 times that of water, the parabolic temperature profile had its maximum at the channel rim and minimum where the interface intersected the plane (Fig. 3). This temperature profile gave rise to thermocapillary flow from the channel rim towards the plane, but at the intersection of the interface and plane, the colder, and therefore lighter, water had to penetrate the heavier water below the interface. This penetration was resisted by buoyancy. The ratio of the maximum thermocapillary flow toward the plane from the rim to the flow perpendicular to the interface ranged from 260 to 835 in the series of experiments. As a result, in each experiment, there was a return flow below the interface from the central plane toward the rim. The oppositely directed thermocapillary and return flows interacted to give rise to mixing and the resulting uniform-temperature layer (see Fig. 3). We note that since buoyancy-driven convection was not possible, the thermocapillary convection did not give rise to fluid motion in the bulk liquid phase of the type normally associated with Marangoni-Bénard convection [4]. The fluid velocity below the uniform-temperature layer, $\boldsymbol{\nu}^L$, was assumed to be that produced by the syringe pump.

At the interface, there was a temperature discontinuity, with the temperature in the vapor greater than that in the liquid. The magnitude of the temperature discontinuity increased with the evaporation flux. However, at a given evaporation flux, the magnitude of the temperature discontinuity was less than that at a spherical interface. For example, at an average evaporation flux of 3.42 g/(m^2 s), at the spherical liquid-vapor interface, the temperature discontinuity was 4.55 °C and the interface curvature was 0.151 mm^{-1}. Whereas when the evaporation flux was 3.48 g/(m^2 s) at the cylindrical interface, the temperature discontinuity was 2.07 °C and the curvature of the cylindrical interface was 0.109 mm^{-1} in one direction and zero in the other. This comparison suggests that the temperature discontinuity is smaller at a interface with smaller curvature. A recent analysis based on classical kinetic theory [25] suggested that the temperature discontinuity should be smaller at an interface of smaller curvature. A cylindrical interface was not explicitly treated in [25], but the comparison suggests a sensitivity of the temperature discontinuity to curvature.

These authors also suggests that statistical rate theory does not give an expression for the energy flux at the interface; however, we note that in the analysis that we performed, the energy flux from the liquid to the vapor phase is taken to be $j_{ev}(h^V - h^L)_I$ where j_{ev} is predicted from statistical rate theory. This expression introduces no adjustable parameters—unlike classical kinetic theory [25]—and gives a quantitative expression for the energy flux that appears in agreement with the measurements (see below).

Below the uniform-temperature layer, the temperature profile was linear with depth (see Fig. 2). The energy flux vector $(n^L h^L \boldsymbol{\nu}^L - \kappa^L \boldsymbol{\nabla} T^L)_I$ was used in the analysis [see Eq. (9)] to determine the energy flux to the bottom of the uniform-temperature layer. Since the system was operating in steady state, it was assumed that this energy was transported across the uniform-temperature layer to the interface by mixing. When the principles of energy and molar conservation were applied to an element of the interface, Eq. (13) was obtained, and when this equation was integrated over the interface—for the nonturbulent experiments—Eq. (16) was obtained. The left-hand side of the latter equation defines the energy required to evaporate the liquid at the measured rate and the right-hand side the energy transported to the interface by thermal conduction and by thermocapillary convection.

The error bars assigned to the measurements were determined from Eq. (16). The value of the error in c_σ was taken to be the same as that determined in [3], ±2.5%. As may be seen in Fig. 5, all of the measurements were within the error bars. Since the area of the interfaces in these experiments was (on average) 4.4 times larger than that of the spherical interfaces used to measure c_σ initially [3] and the energy transport by the thermocapillary energy transport was up to a total of 50% of the total, the agreement seen in Fig. 5 indicates that the error in c_σ was no more than ±2.5%.

The value of c_σ was examined in a second way: taking the value of c_σ to be 30.6 kJ/(m^2 K), the local evaporation flux j_{ev} was calculated from Eqs. (13), (15), (18), and (19) to obtain the results shown in Fig. 7; statistical rate theory was then used with these values of j_{ev} to determine the local pressure on the interface (Fig. 8). We note that this implicitly

assumes that the energy flux from the liquid to the vapor is $j_{ev}(h^V - h^L)_I$. The mean value of the local pressures was calculated, and as seen in Fig. 9, no disagreement was found between the measured pressure in the vapor phase and the mean of the predicted local pressures. Although the predicted gradient in pressure was small, it was consistent with what one would expect on the basis of thermocapillary convection. The agreement between the measured and calculated pressures also supports the hypothesis that c_σ is a property of the liquid-vapor interface and that its value is near 30.6 kJ/(m^2 K) for the interfacial temperature range considered in these experiments. This agreement indirectly supports the expression for the energy flux being $j_{ev}(h^V - h^L)_I$.

We note that statistical rate theory has been previously used to predict the pressure at which a liquid evaporates [7,9] or condenses [6] at a particular rate. In those studies evaporation or condensation took place at a spherical interface and the mean evaporation flux was calculated by dividing the measured evaporation rate by the interfacial area. The temperature on the center line of the spherical interface, which was subsequently found to be the position of the minimum temperature [2], and the calculated mean flux were used in statistical rate theory to calculate the vapor-phase pressure. For the spherical interface, very good agreement was found between the measured vapor-phase pressure and that predicted for evaporation of three different liquids (including water) and the condensation of water. However, for evaporation from a cylindrical interface as indicated by Fig. 7, the evaporation flux is strongly position dependent and assuming a uniform flux would not have been valid in this case.

Since statistical rate theory indicates the evaporation flux depends strongly on the vapor-phase pressure [11], one might have expected that the predicted vapor-phase pressure would have been the inverse of the evaporation flux (Fig. 7), but this conjecture would have ignored the interfacial temperature profile. As seen in Fig. 3, the temperature was also a maximum near the stainless-steel mouth opening. The net result is that the vapor-phase pressure is almost uniform, but is slightly larger at the maximum radial distance from the central plane of the cylindrical interface. This seems a reasonable result, since the thermocapillary flow was toward the central plane of the cylindrical interface; thus, the flow of the vapor would also have been expected to be in that direction.

The volumetric specific heat for bulk water at 0 °C is 4.23×10^3 kJ/(m^3 K). Although this value can not be compared quantitatively with the inferred value of the surface-thermal capacity at present [3], arguments could be advanced to suggest that the proposed value of c_σ is larger than would be expected, at least at an equilibrium interface. In [3], a qualitative argument is offered to suggest that the larger than expected value of c_σ arises from the hydrogen bonding of water as described in the random network model [26–28] that has been shown to account qualitatively for certain surface properties of water [28]. A necessary condition for the validity of the argument advanced in [3] is that c_σ has the same value at a larger-sized interface. The results found in this study satisfy this condition. A second necessary condition for the hydrogen-bonding explanation to be valid is that c_σ has a similar, larger-than-expected value for other hydrogen bonding liquids. This condition has been examined by determining the value of c_σ for D_2O [29]. It is found to share many the characteristics of c_σ for H_2O and to be only slightly larger.

ACKNOWLEDGMENTS

This work was supported by the Alexander von Humboldt Foundation of Germany, the Canadian Space Agency, the Natural Sciences and Engineering Research Council of Canada, and FAU Erlangen-Nürnberg. The experiments were performed at the Institute of Fluid Mechanics, Friedrich-Alexander-University, Erlangen-Nürnberg, Germany. The authors thank Vivek Kumar of this institute for his assistance.

[1] J. R. A. Pearson, J. Fluid Mech. **4**, 489 (1958).
[2] C. A. Ward and Fei Duan, Phys. Rev. E **69**, 056308 (2004).
[3] Fei Duan and C. A. Ward, preceding paper, Phys. Rev. E **72**, 056302 (2005).
[4] An-Ti Chai and N. Zhang, Exp. Heat Transfer **11**, 187 (1998).
[5] J. Willard Gibbs, Trans. Conn. Acad. Arts Sci. **3**, 108 (1876); in *The Scientific Papers of J. Willard Gibbs*, edited by H. A. Bumstead and R. G. Van Name (Dover, New York, 1961), Vol. 1, p. 219.
[6] C. A. Ward and D. Stanga, Phys. Rev. E **64**, 051509 (2001).
[7] C. A. Ward and G. Fang, Phys. Rev. E **59**, 429 (1999).
[8] G. Fang and C. A. Ward, Phys. Rev. E **59**, 417 (1999).
[9] G. Fang and C. A. Ward, Phys. Rev. E **59**, 441 (1999).
[10] A. J. H. McGaughey and C. A. Ward, J. Appl. Phys. **93**, 3619 (2003).
[11] P. Rahimi and C. A. Ward, Int. J. Heat Mass Transfer **47**, 877 (2004).
[12] C. A. Ward, J. Non-Equilib. Thermodyn. **27**, 289 (2002).
[13] C. A. Ward, J. Chem. Phys. **67**, 229 (1977).
[14] C. A. Ward, R. D. Findlay, and M. Rizk, J. Chem. Phys. **76**, 5599 (1982).
[15] C. A. Ward, J. Chem. Phys. **79**, 5605 (1983).
[16] C. A. Ward and M. Elmoselhi, Surf. Sci. **176**, 457 (1986).
[17] C. A. Ward, M. Rizk, and A. S. Tucker, J. Chem. Phys. **76**, 5606 (1982).
[18] J. A. W. Elliott and C. A. Ward, J. Chem. Phys. **106**, 5667 (1997).
[19] J. A. W. Elliott and C. A. Ward, J. Chem. Phys. **106**, 5677 (1997).
[20] J. A. W. Elliott and C. A. Ward, in *Equilibria and Dynamics of Gas Adsorption on Heterogeneous Solid Surfaces*, edited by W. Rudzinski, W. A. Steele, and G. Zgrablich (Elsevier, Amsterdam, 1997), Vol. 104, p. 285.
[21] S. Popov, A. Melling, F. Durst, and C. A. Ward, Int. J. Heat Mass Transfer **48**, 2299 (2005).
[22] A. J. Wheeler and A. R. Ganji, *Introduction to Engineering*

Experimentation (Prentice-Hall, Upper Saddle Raver, NJ, 1996), p. 168.
[23] J. R. Taylor, *An Introduction to Error Analysis: The Study of Uncertainties in Physical Measurements*, 2nd ed. (University Science Books, Sausalito, CA, 1997), p. 187.
[24] G. Herzberg, *Molecular Spectra and Molecular Structure* (Van Nostrand, Princeton, NJ, 1964), Vol. 2, p. 281.
[25] M. Bond and H. Struchtrup, Phys. Rev. E **70**, 061605 (2004).
[26] S. A. Rice and M. G. Sceats, J. Phys. Chem. **85**, 1108 (1981).
[27] A. R. Henn and W. Kuzmann, J. Phys. Chem. **93**, 3770 (1989).
[28] A. R. Henn, Biophys. Chem. **105**, 533 (2003).
[29] Fei Duan and C. A. Ward, following paper, Phys. Rev. E **72**, 056304 (2005).